Nanoscale Coordination Polymers for Medicine and Sensors

Rubén Solórzano,[a,b] Salvio Suárez-García,[a] Fernando Novio,[a,b] Julia Lorenzo,[c] Ramon Alibés,[b] Félix Busqué,[b] Daniel Ruiz-Molina[a]*

[a]*Catalan Institute of Nanoscience and Nanotechnology (ICN2), CSIC and BIST, Campus UAB, Bellaterra, 08193 Barcelona, Spain*

[b]*Departament de Química, Universitat Autònoma de Barcelona (UAB), Campus UAB, Cerdanyola del Vallès 08193, Barcelona, Spain*

[c]*Institut de Biotecnologia i de Biomedicina and Departament de Bioquímica i Biologia Molecular. Universitat Autónoma de Barcelona, 08193 Bellaterra, Barcelona, Spain*

Keywords: nanoparticle, coordination polymer, nanomedicine, sensors, nanoscale

List of Contents

Abstract

Miniaturization of coordination polymers to the nanoscale represents a unique opportunity to assemble a novel class of highly customizable functional materials that marry the rich diversity, chemistry and properties of coordination complexes to the advantages of nanomaterials. The new structures, which exhibit well-defined and dispersed morphologies, can allow for a proper correlation with their functionality, and therefore, enable the rational design of new generations of these nanostructures targeting specific desired properties.

In this Chapter we will give a brief introduction to the rational fabrication of such functional nanostructures following different coordination polymerization mechanisms. The novel "smart" nanoscale coordination polymer particles (NCPs) exhibit interesting properties of relevance for different fields and applications, worth to mention Nanomedicine and Sensors.

Herein we make a summary of the main results obtained in both areas that evidence the significance of this novel family of materials. For this, the review has been divided into two main sections. In the first part we revise general methodologies for cargo loading and delivery, including the design of stimuli-responsive systems. In the second section we will review the latest advances in the use of NCPs as chemical sensing platforms. These results open new avenues for all the possible applications that can be derived from the implications of CPPs on surfaces. Finally, a brief introduction to the new research line on 2D-coordination polymers will be outlined.

1. Introduction

The self-assembly of coordination polymers (CPs) at the nanoscale represents a novel opportunity to develop a unique class of highly tailorable functional materials that combines the rich diversity of CPs with the advantages of nanomaterials. The synthetic flexibility of directional metal-ligand bonds is used to systematically control and tune the chemical topology, nanodimensions and morphologies of the corresponding materials. The limitless choice of metallic elements ensures a broad range of interesting magnetic, electronic, optical, and catalytic properties. And finally, miniaturization to the nanometer scale improves their colloidal stability, increases the surface area (and therefore the catalytic, sensing or storage capabilities) and is used to systematically fine-tune the physical properties of the materials. All of these advantages are highly required for most envisioned applications.[1]

So far, two main families of CPs at the nanoscale have been described:

- Amorphous coordination polymer nanoparticles, referred from now on as nanoscale coordination polymers (NCPs),[2] also called infinite coordination polymers (ICPs)[3] or coordination polymer particles (CPPs).[4]
- Nanoscale crystalline and porous coordination polymer structures, from now on NMOFs.

NMOFs exhibit exceptionally high surface areas and loading capacities while allow for control over the release of cargo via modification of tunable pores. The crystalline nature of MOFs also facilitates analyses of host–guest interactions and therefore a systematic design and optimization of drug encapsulation and release studies. As a result of these interests, several comprehensive reviews summarizing progress in MOFs for applications are available elsewhere,[5] being the nanomedicine of the emerging areas of interest over the last years.[6] On the other hand, NCPs have emerged as an alternative to NMOFs. This new family of nanoparticles are amorphous with spherical morphologies ranging from a few to hundreds of nanometers in size. The most common synthetic approach to obtain NCPs is mixing metal ions and the corresponding organic ligands in the presence of a poor solvent that induces a fast precipitation, i.e. using out-of-equilibrium conditions.[7] To minimize the interfacial free energy between the surface of

the NCPs and the solvent during the reaction, the nanoparticles acquire the spherical shape. Other approaches to obtain NCPs have been described:[8] worth to mention are reverse micro-emulsions,[9] lab-on-a-chip implementation[10] and Dip-Pen Nanolithography (DPN).[11]

Since first reported in 2005 by Mirkin[12] and Wang,[13] the number of publications related with NCPs is growing exponentially along with the variety of applications exemplified, including heterogeneous catalysis,[14] spin-crossover,[10,15] separation of oils from water,[16] bio-sensing,[17] pH sensors,[18] gas absorption systems,[19] hybrid nanoparticle-based devices,[20] fluorescent sensors,[21] precursors for inorganic particles[22] and thermochromic nanostructures.[23] Especial mention deserves the application of NCPs in medicine. With this aim, drugs can be trapped as constitutive building blocks of the polymeric unit (chemical entrapment) or through the physical encapsulation inside the nanoparticle.[24] Physical encapsulation of active substances such as organic dyes, magnetic nanoparticles, or luminescent quantum dots was already reported back in 2009.[25] One year later, the same authors showed that these capsules not only can encapsulate but also can release active principles as polymeric nanoparticles do.[25] On the other side, chemical entrapment allows for a better fine-tuning of the release kinetics (up to many hours) as well as better formulation with increased encapsulation yields. The use of active metal drugs, such as Pt(IV),[26] as polymeric nodes of coordination polymers represents the most successful example of chemical entrapment. Less explored has been the chemical entrapment through tethering of active drugs as chelating ligands, in spite of the fact that its efficiency has already been reported.[27] Moreover, the chemical flexibility of organic synthesis may allow for the design of drugs (ligands) cleaved under physiological conditions.[28] Together, encapsulation capabilities, nanodimensions and excellent colloidal and chemical stabilities have allowed for their use in medical applications.

Beyond their use in Nanomedicine, the scope of application of NCPs nanoparticles as platforms for chemical sensing has also grown exponentially in the last years.[28] Lanthanide-based NCPs nanoparticles constitute the main class of these nanostructures used as sensors for different chemical species, based on its performance in enhancing or quenching the fluorescence of a sample in the presence of a certain analyte.

Herein we make a summary of the main results obtained in both areas that evidence the significance of this novel family of materials. For this, the review has been divided into two main sections. In the first part we revise general methodologies for cargo loading and delivery, including the design of stimuli-responsive systems. In the second section we will review the latest advances in the use of NCPs as chemical sensing platforms. Rather than a detailed list of examples and specific cases reported so far, it is our aim to go deeper into the mechanistic details of their behavior.

2. Nanoscale Coordination Polymers for Drug Delivery

2.1. Encapsulation and release approaches

As mentioned above, cargo loading is accomplished either via direct incorporation of active drugs as NCPs building blocks (metal ions or organic ligands) or via guest encapsulation during NCPs synthesis or in a post-synthetic step. Following this approach we can achieve high drug loadings, although the morphology and physicochemical properties are difficult to control. Using the second approach, we have more control over the morphology but overall the active drugs are incorporated in lower amounts and their loading strongly depends on the physicochemical properties of each drug (leakage can occur). Amorín-Ferré et al. illustrated the differences between both encapsulation approaches and their drug release kinetics (Figure 1).[24] NCPs composed by Co(II), 1,4-bis(imidazol-1-ylmethyl)benzene (bix) and 3,5-di-*tert*-butylcatechol, were formed in the presence of fluorescent compounds, either containing a free chelating catechol (coordination to the main backbone takes place) or a protected one (physical entrapment). Cargo loading via direct attachment to the NCPs framework, was slowly released only upon particle degradation, whereas the encapsulated one was easily released through a diffusion mechanism. On the other hand, Novio et al. reported the formation of catechol-iron based NCPs containing carboxylic groups as platforms for further functionalization via condensation reactions.[29] As a proof-of-concept, the particles were covalently labelled with bioactive functional moieties as a fluorescent dye or polyethylene glycol (PEG). The particles showed efficient cellular uptake and no

significant cytotoxicity. Their use as drug delivery platforms was then modeled by encapsulating the anticancer drug camptothecin, showing an improvement in IC_{50} values as compared with the free drug.[29]

Insert Figure 1 here

Figure 1. (a) Chemical structures of fluorescent guest compounds **1** and **2** used in the formation of structural-analogous of **M1** and **M2** particles, used to investigate degradation and diffusion-controlled release in NCPs. (b and c) SEM (left) and TEM (right) images of **M1** (b) and **M2** (c) particles. Scale bars for SEM are 1 μm and 200 nm for TEM. (d) Release profiles of fluorescent guest molecules from **M1** (□) and **M2** (○) at 37 °C, averaged over four independent experiments. Reproduced from reference 24 with permission of the copyright holder.

Liang et al. synthesized nanowire coils of organometallic coordination polymers by using the emulsion polymerization technique.[30] The nanowires were formed by the self-assembly of a triblock copolymer terminated with a complex of β-cyclodextrin and 4,4'-bipyridine and their subsequent polymerization using Ni(II). The resulting material was able to incorporate hydrophobic organic cargoes, as showed by the encapsulation of model hydrophobic dye Nile red. Li et al. reported nanostructures made by the self-assembly of curcumin, amino acids and Zn(II).[31] The nano-structuration of the curcumin molecule helped to overcome its quick degradation in physiological media. Additionally, tumor accumulation and inhibition was enhanced when curcumin was delivered as NCPs. Li et al. illustrated the feasibility of NCPs for macromolecule delivery with the report of iron-induced DNA self-assemblies.[32] The resulting nanostructures could be fine-tuned by modifying the Fe/nucleotide ratio or their concentration during the reaction mixture. Although DNA is unable to penetrate cell membranes, its nanoassembly allowed an efficient cellular uptake, reported mainly in endosomes or lysosomes. In vitro and in vivo studies showed the potentiality for DNA delivery using CpG, an immune stimulatory DNA.

Fan et al. developed an interesting strategy for monitoring drug release in real time based on the self-assembly of a tryptophan-phenylalanine dipeptide with Zn(II) ions to form dipeptide nanoparticles (DNPs).[33] DNPs were found to display fluorescence in the visible range and possessed advantages over organic fluorophores, quantum dots or

green fluorescent proteins like photo- and thermal stability, biocompatibility and narrower emission bandwidth. Conjugation of the chemotherapeutic drug doxorubicin through π-π stacking, afforded DNPs able to experience release (50% in 24 h, pH 6.0), which could be then monitored in vitro due to their fluorescent properties. Bertleff-Zieschang et al. described an approach for the coordination-driven assembly of different flavonoids and Fe(III) ions, which could be either used for the preparation of films or microcapsules after template removal.[34] The resulting structured flavonoids displayed higher antioxidant activity than in the free form and was preserved over multiple scavenging cycles.

2.2. Stimuli-responsive delivery platforms

The high degree of tune ability in the design of NCPs allows the fabrication of materials with responsive properties. Several examples have been reported in which an external stimulus is able to trigger a more controlled drug delivery. Probably the most relevant stimulus is pH, because of both the pH-dependence nature of coordination bonds and the relevance of pH variations within intra- and extracellular environments. Other potential stimuli for cargo release might include redox- or light-responsive materials.

pH-responsive

Gao et al. reported nanoparticles composed by the self-assembly of iron ions and 1,1'-(1,4-butanediyl)bis(imidazole) and the subsequent encapsulation of doxorubicin hydrochloride (40% drug loading content) followed by silica coating.[35] Interestingly, these particles exhibited sustainable drug release for several days, which was significantly faster at pH 5.0 than under physiological conditions. Another example of pH-dependent doxorubicin delivery using NCPs was reported by Bai et al.[36] In this work, a triblock copolymer composed by poly(ethylene glycol)-b-poly(2-hydroxyethyl methacrylate-Boc-histidine)-b-poly(styrene) (PEG-PBHE-PS) was prepared and self-assembled into micelles. Further polymerization of histidine moieties, doxorubicin and Cu(II) allowed the formation of micelles with a drug loading as high as 26.1%. Due to the pH-dependence of the stability of the coordination bonds between copper, histidine and doxorubicin, drug leakage was strongly suppressed at physiological pH but drug release

was drastically increased at pH 5.0. Further studies using doxorubicin included NCPs composed by an iron(III)-gallic acid network that could potentially encapsulate doxorubicin up to 93.5% drug loading content by its coordination with the Fe(III) centers.[37] In this work, Han et al. showed that these acid-sensitive NCPs allowed a real-time drug release monitoring into lysosomes, as doxorubicin inherent fluorescence was quenched when the polymer was nanostructured but recovered as doxorubicin was released due to the acidity in lysosomes. Moreover, in vivo evaluation showed significant tumor growth inhibition with minimal heart toxicity.

Xu et al. proposed a strategy for releasing Fe-salphen complexes using core-shell nanoparticles composed by a Fe_3O_4 core and a salphen-In(III) coordination polymer shell.[38] Using this approach, the polymeric shell was observed to rapidly hydrolyze at pH 5.0, while the Fe_3O_4 core slowly collapsed to release iron ions chelated by salphen and form the active therapeutic species. In vitro studies determined significant selectivity for cancer cells and IC_{50} values comparable to those of pharmaceutically-active Mn(II)-salen complexes.

Wang et al. exploited the lability of metal-ligand bonds to cap titanium nanotubes (TNTs) containing antibacterial agents using coordination polymers.[39] In this work, TNTs were loaded with model drugs ibuprofen, vancomycin or Ag nanoparticles and then capped by the bix ligand and Zn(II) or Ag(I) ions. At physiological pH, drug release was found to be blocked, however it increased as pH decreased, due to the degradation of the coordination polymer. In addition, metal ions could offer favorable biological functions: Zn(II) could promote the proliferation of osteoblastic cells while Ag^+ exhibited antibacterial properties.

Ejima et al. took advantage of the pH dependency in Fe(III)-catechol coordination by preparing coatings based on the polymerization of tannic acid with iron(III) ions.[40] The authors reported a general approach for the one-step formation of films in a wide variety of substrates, including inorganic, organic and biological templates. The capsules formed were observed to disassemble in acidic pH due to protonation of catechol moieties and therefore destabilization of cross-links. In addition, cytotoxicity was not observed in any iron-tannic acid coating tested. In a follow-up study, the authors also described a multistep assembly of iron(III)-tannic acid which exhibited different

properties than the ones made by one-step deposition, e.g. permeability, stiffness or degradability.[41] Their pH-responsiveness was further exploited in the formation of doxorubicin-loaded metal-phenolic microcapsules using mesoporous $CaCO_3$ particles as sacrificial templates.[42] Capsules were prepared by the polymerization of tannic acid with Al(III), although Mn(II) and Gd(III) were also used for potential theranostic applications. As expected, their disassembly was observed to be pH-dependent, being relatively stable at pH 7.4 but degraded in a significant amount (80%) during 48 h at pH 5.0. In vitro assays also showed efficient capsule internalization and intracellular drug release, as well as comparable or even improved, in some cases, therapeutic effects. Moreover, encapsulation of other drugs such as irinotecan, topotecan or verapamil, was also proven in an analogous way.[Ref?] The same strategy was followed by Ju et al. using a mixture of catechol-functionalized hyaluronic acid and polyethyleneglycol instead of tannic acid.[43] The resulting doxorubicin-loaded material showed an acid-triggered drug release along with enhanced targeting for CD44+ cancer cell line instead of CD44- cells due to the presence of hyaluronic acid and polyethyleneglycol. A further study showed the benefits of protein corona in such systems, improving target specificity.[44] In a subsequent study, Park et al. used the previous approach to coat individual yeast cells.[45] Coated cells were found to retain their metabolic activities and viability, as well as an enhanced protection against binding of *E. Coli*, UV-C irradiation, lyticase and silver nanoparticles. Due to the pH-sensitive nature of their coating, cells could also be both preserved and exposed on-demand. Catechol-iron coordination was also used by Besford et al. to coat oleic acid nanoemulsions with a crosslinking of catechol-containing polyethyleneglycol and Fe(III) ions.[46] The resulting doxorubicin-loaded nanostructures displayed an acid-induced drug release behavior. In vivo assays showed a stealth-like response with regards to cell association and a blood circulation half-life of 50 min. In vitro tests revealed significant cytotoxicity against human breast cancer cells, demonstrating successful cell internalization and intracellular release of the drug.

Huang et al. recently reported the synthesis of Zn-based hexahistidine-metal nanoassemblies (HmA) for drug encapsulation.[47] Such assemblies exhibited interesting properties such as an average size of 60 nm, the possibility of encapsulating from small molecules (fluorescein) to polymers (dextran-40k) and a loading capacity of up to 53%.

Moreover, a pH dependence was reported, with a burst release at pH 4.5 in minutes and a slow release at neutral pH. Minimal cytotoxicity and fast internalization were also reported for the HmA. In addition, encapsulation of the chemotherapeutic drug camptothecin improved the antitumor activity compared to the free drug.

Not only coordination bonds within NCPs can trigger a pH-dependent response, but also the NCPs ligand design. As a proof-of-concept, Nador et al. compared the pH-responsiveness of two structurally analogous bis(catechol)-based cobalt NCPs, containing either an imine functionality or an alkyl chain.[18] Notably, NCPs composed by the imine-containing linker showed a loss of their spherical shape and aggregation at pH 5.0, in addition to the disappearance of the characteristic imine infrared bands. However, NCPs treated at neutral pH preserved their morphology and chemical composition. Likewise, NCPs composed by the alkyl chain based linker confirmed the role of the imine moiety in the nanostructure disassembly, as they displayed great stability independent of the pH value used. Further examples include the nanostructures designed by Liu et al. based on Hf(IV) and an imine-based acid sensitive linker that were used for the encapsulation of the chemotherapeutic drug chloro(triphenylphosphine)gold(I) (TPPGC).[48] These particles exhibited excellent stability at physiological pH but rapidly collapsed in mild acidic environments to release their cargo. In vitro and in vivo studies examined the feasibility of this system as combinational chemo-radiotherapy, due to the mixture of the encapsulated chemotherapeutic drug and hafnium ions that act as radio-sensitizers, showing an improvement as compared with conventional chemotherapy or radiotherapy. In addition, these nanostructures displayed no significant toxicity and their biodegradability could potentially avoid long-term toxicity concerns. In another study, Liu et al. further exploited this idea by encapsulating collagenase using a self-assembly between the previous imine-based acid sensitive linker and Mn(II) ions.[49] After its PEGylation, these NCPs showed a similar pH-dependence than those of the previous work, being stable at neutral pH to degrade under acidic environments. In vivo studies demonstrated efficient accumulation within tumors. In addition, the released collagenase would allow an enhanced retention and permeation of a second wave of

therapeutic nanoparticles (chlorin e6 (Ce6)–loaded liposomes) which lead to an improved photodynamic therapeutic effect.

Yang et al. described a series of nano-constructs formed by a dicarboxylic cisplatin (IV) prodrug, poly-L-histidine-PEG and a metal cation (Ca(II), Co(II), Ni(II), Hf(IV), Tb(III)).[50] In this case, the NCPs experimented a charge conversion from slightly negative to positive upon a pH decrease from physiological to pH 5.5. Thus, these nanoparticles were stable under pH 7.4 but experimented a rather fast drug release at acidic pH. Such behavior was rationalized by the weakening of the histidine-metal bond by protonation of imidazole groups and further network collapse. Therapeutic efficacy of these NCPs were tested in vitro and in vivo, showing tumor suppression efficacy under relatively low drug doses.

Wang et al. reported a concept of pH-responsive NCPs based on the coordination of Cu(II) and an organic linker containing the macrocycle dioxocyclam.[51] In this approach, particles were formed by solvent-assisted precipitation of the corresponding soluble Cu(II)-linker. Upon a pH decrease, the dioxocyclam-Cu(II) complex was dissociated as the macrocycle was protonated, leading to the disassembly of the nanostructure. Interestingly, this work also demonstrated polymer collapse upon the addition of a competitive copper chelator (EDTA) at neutral pH.

2.3. Other stimuli

Concerning the use of other stimuli in NCPs, several examples have been recently reported. For instance, Zhang et al. developed a simple method for the fabrication of photodegradable nanostructures based on the self-assembly of Zn(II) and a bis(imidazole) ligand containing a photocleavable *o*-nitrobenzyl unit.[52] These structures exhibited the capability to physically encapsulate different cargoes. Specifically, fluorescein, the antibiotic agent tetracycline or the chemotherapeutic drug doxorubicin, were separately encapsulated within the polymer network. Interestingly, their release in aqueous solution was significantly increased upon UV light irradiation when compared with no irradiated samples. In addition, in vitro experiments using HeLa cells showed no significant cytotoxicity for the non-loaded NCPs, while doxorubicin-loaded

NCPs retained a cytotoxic effect which became more evident upon irradiation, suggesting an enhanced drug release into the cells under these conditions. Liu et al. reported a strategy for light-controlled drug release based on Hf(IV) following an analogous approach to that used in the fabrication of a pH-sensitive NCPs for combinational chemo-radiotherapy.[53] In this case, nanostructures were formed by the polymerization of a bis-(alkylthio) alkene linker (BATA), a singlet-oxygen sensitive ligand, and Hf(IV) cations. After loading with both photosensitizer chlorin e6 and chemotherapeutic drug doxorubicin, these NCPs were able to produce singlet oxygen upon red light irradiation, thus inducing drug release due to BATA cleavage and collapse of the nanoparticle. Notably, CT imaging and biodistribution measurements showed efficient tumor accumulation, while presenting an improvement for combined chemo-photodynamic therapy and reduced toxicity when compared with the free drugs (Figure 2). Hu et al. synthesized novel NCPs based on photochromic ligands for the potential encapsulation/release of cargoes upon light irradiation.[54] In this study, microparticles formed by Zn(II) and a carboxylic-functionalized diarylethene photoswitch exhibited reversible photochromic behavior in the solid state and in solution. Remarkably, their change in surface area, pore shape and size upon interconversion by UV or visible light could provide a novel approach for light-triggered cargo release.

Insert Figure 2 here

Figure 2. (a) Schematic illustration for the synthesis of NCP-Ce6-DOX-PEG nanoparticles (b) TEM images of NCP-Ce6-DOX-PEG before and after light irradiation. (c) Sustained release of Ce6 and DOX from NCP-Ce6-DOX-PEG with or without 660 nm LED light exposure at the power density of 5 mW cm^{-2}. (d) Tumor growth curves of mice in different groups after receiving various treatments. Reproduced from reference 53 with permission of the copyright holder.

Cherepanov et al. reported the redox-dependent disassembly of gallic acid-Fe(III) networks.[55] The authors evaluated the electrochemical reversibility of the system, identified the oxidation state of the redox-active species and showed that release of Fe(III) could be achieved, additionally identifying the specific conditions for "on-off" or continuous disassembly of the networks. Concerning redox-induced disassembly of nanostructures, Buywalda et al. developed micelles based on poly(ethylene glycol)-

poly(N(2-hydroxypropyl)methacrylamide (PEG-P(HPMA)) including hydrophobic 4-(methylthio)benzoyl side groups that could be crosslinked using the metal-organic linker [ethylenediamineplatinum(II)]$^{2+}$.[56] As a proof-of-concept, curcumin was encapsulated in such micelles with and without crosslinking. When compared to the free micelles, the crosslinking resulted in a smaller size, a lower critical micellar concentration and a better retention of the encapsulated drug. Drug release was found to be lower in the crosslinked micelles, however it was increased in the presence of dithioerythritol, which mimicked the presence of glutathione in the intracellular environment.

2.4. Multi stimuli-responsive systems

Li el al. reported a simultaneously pH- and glutathione-responsive nanoparticles composed by the self-assembly of Zn(II) and a histidine containing dipeptide or a amphiphilic histidine derivative (Figure 3).[57] Moreover, the model drug chlorin e6 could be incorporated in loading capacities higher than 50% through cooperative coordination with the peptide and Zn(II). Importantly, the nanostructures displayed robust stability in physiological conditions but experimented a burst release upon either a pH decrease or a glutathione concentration increase. Owing to these features, these NCPs presented prolonged blood circulation lifetime, enhanced accumulation in tumors, improved antitumor efficacy compared to non-encapsulated photosensitizers and negligible in vitro or in vivo toxicities.

Insert Figure 3 here

Figure 3. (a) Construction of metallo-nanodrugs through cooperative coordination of small peptides and photosensitizers (Ce6) in the presence of zinc ions. (b) SEM images of the metallo-nanodrugs. (c) Schematic illustration and pictures showing the ultrasensitive response of Fmoc-H/Zn^{2+} to pH and GSH changes. (d) Ce6 release profiles from Fmoc-H/Zn^{2+}/Ce6 in different release buffers. Unencapsulated Ce6 was used as a control group. The lines are the fitted results according to the Gompertz kinetic release model. Error bars denote the standard deviation (n = 3). *P < 0.05 (one-way ANOVA). (e) Fluorescence images showing that Fmoc-H/ Zn2+/Ce6 and Z-HF/Zn2+/Ce6 allow better accumulation of Ce6 in tumor sites than unencapsulated Ce6. Reproduced from reference 57 with permission of the copyright holder.

Another example of multistage responsiveness was reported by Liu et al.[58] In this work, MnO$_2$ nanoparticles stabilized by bovine serum albumin were prepared and coated with

a shell composed by the polymerization of Hf(IV) and c,c,t-(diamminedichlorodisuccinato)Pt(IV) (DSP), a cisplatin prodrug. After a PEGylation step, the formed nanocomposite could act as a radio-sensitizer due to the presence of hafnium ions, as chemotherapeutic agent resulting from cisplatin release under reductive environments upon cell uptake or as magnetic resonance imaging contrast owing to the decomposition of MnO_2 in the acidic tumor environment. In addition, MnO_2 could trigger decomposition of tumor endogenous H_2O_2 improving hypoxia-associated radiotherapy resistance. As a result of these factors, an efficient in vivo chemo-radiotherapy was observed while the inherent biodegradability of NCPs and MnO_2 lead to efficient excretion the nanocomposites with no appreciable toxicity.

Wang et al. described an interesting example of drug release triggered by cellular endogenous species.[59] Specifically, the authors designed a folic acid-PEG-poly(4-vinylpyridine)-Ir(III)-2-phenylquinoline complex that self-assembled in water to form core-shell spherical nanoparticles with an average radius of 25 nm. Within this nanostructure, the Ir(III)-containing moiety acted as the core, whereas PEG remained in the shell. Remarkably, in vitro experiments revealed the interaction of intracellular histidine with the nanoparticles in order to release the iridium complex $[Ir(pq)_2]^+$ (pq = 2-phenylquinoline), which served both as drug and as precursor of a phosphorescent emitter, thus enabling not only intracellular drug release but also phosphorescent tracking of its cellular internalization.

The possibility of fine-tune and rationalize NCPs composition also allows the formation of multi-responsive systems that act as molecular logic gates. Pu et al. illustrated such behavior in nanostructures composed by the self-assembly of Tb(III) or Eu(III) ions and the nucleotide guanosine 5'-monophosphate (GMP).[60,61] These nanoparticles, after the encapsulation of *N*-methyl mesoporphyrin IX (NMM), exhibited fluorescence emission that could be described as the output of different binary logic gates when two or three distinct stimuli (inputs) were applied. Therefore, this input-dependent encapsulation could be used for controlled release and, simultaneously, cellular imaging. Gao et al. also reported GMP-lanthanide assemblies that could respond to several external stimuli such as dipicolinic acid, ethylene diamine tetraacetic acid, pH and Cu(II) or Hg(II) ions.[62] In a similar way, Bai et al. described the core-cross-linking of a disulfide-containing

doxorubicin prodrug with Cu(II) to form nanoparticles that acted as an AND logic gate, i.e., output is released only if both inputs are present.[63] In this example, inputs corresponded to acidic and reductive conditions, commonly found in cancer cells. Thus, premature drug release was observed to be suppressed under neutral and non-reductive environments, but enhanced when both conditions, low pH and reducing agents, were accomplished.

3. Nanoscale Coordination Polymers for Chemical Sensing

The scope of application of NCPs as platforms for chemical sensing has also grown exponentially in the last years. Lanthanide-based NCPs nanoparticles constitute the main class of these nanostructures used as sensors for different chemical species, resting its performance in enhancing or quenching the fluorescence of a sample, in the presence of a certain analyte. In turn, Terbium (III) is the most common lanthanide ion used.[64-78]

Tb(III) nanosensors, based on an enhancement of the fluorescence, can operate following three different mechanisms: i) by suppression of the inhibition of Tb(III)-ligand network fluorescence;[64,65] ii) by sensitization of Tb(III) fluorescence;[66,67] and iii) through the releasing of a fluorescent dye.[68-70] Among the examples working by suppression of the inhibition of Tb(III)-ligand network fluorescence, Chen and coworkers demonstrated the utility of NCPs composed of Tb(III), adenine (Ad) as main constitutive ligand, and dipicolinic acid (DPA) as an auxiliary ligand sensitizer of the fluorescence of the metal, as a fluorescence nanosensor for Hg(II) (Figure 4).[64] The fluorescence of the NCP network is very low due to a photoinduced electron transfer (PET) from adenine to DPA which avoids the expected intramolecular energy transfer from this molecule to Tb(III) that otherwise sensitizes the fluorescence of this atom. In the presence of Hg(II) a significant enhancement of fluorescence takes place due to the disappearance of the PET process as a consequence of the coordination of this metal to adenine. As nanosensor for Hg(II), it presents a remarkable sensitivity and range of application between 0.2 to 100 nM.

Inset Figure 4 here

Figure 4. The use of Tb(III) Coordination Polymer Nanoparticles for mercury(II) sensing constitutes a paradigmatic example of using the enhancement of fluorescence in presence of an analyte for sensing purposes. In this case, a suppression of the inhibition of Tb(III)-ligand network fluorescence in the presence of Hg (II) takes place. The fluorescence of the NCP network is very low due to a photoinduced electron transfer (PET) from adenine to DPA which avoids the expected intramolecular energy transfer from this molecule to Tb(III) that otherwise sensitizes the fluorescence of this atom. In the presence of Hg(II) a significant enhancement of fluorescence takes place due to the disappearance of the PET process as a consequence of the coordination of this metal to adenine. Reproduced from reference 64 with permission of the copyright holder.

A similar strategy based on the enhancement of fluorescence of NCPs composed of Tb(III) ions has been described by Shi and coworkers for the selective sensing of biothiols, hydrogen peroxide or glucose in solution.[65] The nanoparticles are made with Tb(III), the nucleotide guanosine monophosphate (GMP) as bridging ligand and Hg(II) which interacts with GMP and quenches the fluorescence of the Tb-GMP network. The as-prepared Tb–GMP–Hg nanoprobe can be used for the "turn on" fluorescent determination of several biothiols (Cys: cysteine, Hcys: homocystine, GSH: glutathione), through their high affinity for Hg(II), in a range between 10 and 1000 μM. Moreover, the addition of H_2O_2 reverses the Cys-mediated luminescence increase in the Tb–GMP–Hg probe, originating a "turn off" luminescent assay for H_2O_2 in concentrations between 1 and 200 μM. The Tb–GMP–Hg- Cys material is also suitable for the detection of glucose, through the generation of H_2O_2, if the enzyme glucose oxidase (GOx) is incorporated in the system.

An additional example of enhancing the fluorescence of Tb(III)-based NCPs to constitute an efficient nanoprobe is the reported by Tan et al. for the detection of antibiotic Ciprofloxacin.[66] In this case, the NCP network is formed with Tb(III) and adenine as bridging ligand. A fluorescent emission of Tb(III) occurs in the presence of ciprofloxacin, due to the formation of a complex between this molecule with Tb(III) atoms on the surface on the NCPs. The thus obtained nanosensor presents a range of applications with linear enhancement of fluorescence between 60 nM to 14 μM. In the example presented by Cao and coworkers, the enhancement of fluorescence of NCPs composed of Tb(III) ions and the bis hydrazine of 4-formyl-3-hidroxybenzoic acid (HDBB) as

fluorescent bridging ligand, allowed the development of a fluorescent probe for zinc.[67] The Tb-HDBB network emits fluorescence at 590 nm when excited at 365 nm. Upon the addition of Zn(II), some carboxylic acid groups on the surface of the Tb-HDBB nanoparticles bind to this cation, resulting in the formation of new Tb-HDBB-Zn nanoparticles that present an additional increase in fluorescence emission at 470 nm with a concomitant decrease at 590 nm, providing a probe for the ratiometric assay for Zn(II) in a remarkable wide range from 100 nM to 60 μM.

The last strategy for enhancing the fluorescence of a sample in the presence of an analyte consists of the encapsulation of an adequate dye in the NCPs. Thus, in the work reported by Mao and coworkers, NCPs composed of Tb(III) ions, GMP as constitutive ligand and the encapsulated fluorescent dye 7-amino-4-methyl coumarin, are used as a fluorescent probe for alkaline phosphatase (ALP) activity.[68] The coumarin dye itself emits weak fluorescence while encapsulated, but upon the presence of ALP, the phosphate group in the GMP ligand is cleaved, resulting in the destruction of the Tb-GMP network and the release of encapsulated coumarin dye into solution, causing the decrease in the fluorescence intensity emitted from the Tb-GMP network itself and the increase in the fluorescence intensity emitted from coumarin, providing a probe for the ratiometric assay for ALP in a range from 0.025 U/mL to 0.2 U/mL. Similarly, in a work reported by Ye and coworkers, heterobinuclear NCPs composed of Ce(III) and Tb(III) ions and the nucleotide AMP as constitutive ligand, provided a fluorescent probe for Hg(II).[69] In this case, a fluorescent dye (coumarin) was encapsulated to form nanoparticles which emit characteristic luminescence of Tb(III) at 548 nm after excitation, whereas coumarin itself emits weak fluorescence at 445 nm. In the presence of Hg(II), a strong coordination between AMP and Hg(II) occurs, resulting in the destruction of the Ce-Tb-AMP nanoparticles and the release of encapsulated coumarin dye into solution. As a result of this process, a quenching of the fluorescence intensity emitted from the Ce-Tb-GMP network takes place while increasing the fluorescence intensity emitted from coumarin, providing a double signal based nanoprobe for the ratiometric assay for Hg(II) in a wide range from 0.08 to 1000 nM. Following a closely related strategy, Li and coworkers reported NCPs composed of Tb(III) ions, GMP as binding ligand and an encapsulated NIR fluorescent hemicyanine dye (CyOH) as a fluorescent probe for alkaline phosphatase

(ALP) endogenous activity in biological samples, along with satisfactory tissue imaging capability at the depths of 40-120 μm.[70] In the presence of ALP, phosphate bonds in the Tb-GMP network are cleaved, resulting in the destruction of the nanoparticles and the release of encapsulated CyOH into solution, originating from an increase of fluorescence intensity emitted by this dye that provides a NIR fluorescent nanoprobe for ALP activity in cells, tissues and mice.

On the other hand, the quenching of fluorescence of different atoms in NCPs has been also a recurrent strategy for the development on nanosensors of different chemical species. Thus, Liu and coworkers described the use of NCPs nanoparticles as a tool for selective DNA homopolymers sensing and adsorption.[71] Thus, a series of diverse NCPs between a nucleobase (adenine) or different nucleotides and various metal ions (Au(III) and Tb(III) among others) was prepared and tested for sensing of complementary DNA homopolymers. In the case of using Au(III) and adenine, the corresponding fluorescent NCPs can be used as a sensor for complementary DNA homopolymers due to a linear quenching of the fluorescence of the nanoparticles in a range of DNA concentrations between 5 to 20 nM. A similar strategy based on the quenching of fluorescence of NCPs composed of Tb(III) ions has been described by Song and coworkers for the selective sensing of hydrogen peroxide in biological fluids.[72] The NCP network is formed with Tb(III) phenylalanine as structural ligand and carboxyphenylboronic acid (CPBA) as guest ligand and sensitizer of the Tb(III) fluorescence. In the presence of H_2O_2 the fluorescence of the NPs is quenched as a consequence of oxidative deboronation of CPBA molecules and the corresponding intramolecular charge transfer (ICT) process from the formed 4-oxo anions to the emissive state of lanthanide ions. The fluorescence of the nanosensor decreases linearly with the increase of H_2O_2 concentration from 6 μM to 1 mM and can be used in urine samples. In another example, Wu and coworkers reported the implementation of NCPs of Tb(III) as a selective fluorescent method for the sensing of Cu(II) in rat brain. The NCPs is composed of terbium ion, adenosine monophosphate (AMP) as main constitutive ligand and 5-sulfosalicylic acid (SSA) as an auxiliary ligand sensitizer of the fluorescence of Tb(III).[73] The addition of Cu(II) into a solution of SSA/AMP-Tb nanoparticles strongly quenches the fluorescence because the specific coordination interaction between SSA and Cu(II) makes the energy transfer from SSA to

Tb(III) inefficient. The decrease in ratio of the fluorescence intensity of SSA/AMP-Tb shows a linear relationship for Cu(II) within a concentration range between 1.5 to 24 μM. Eventually, by combining with micro-dialysis techniques, the method resulted successfully in the detection of cerebral Cu(II) in rat brain. Similarly, Chen and coworkers described the quenching of fluorescence of NCPs composed of Tb(III) ions for the selective sensing of nitrite ion (NO_2^-).[74] In this case, the NCP network is formed with Tb(III) 5-fluorouracil as structural ligand and 4,4-oxybis(benzoic acid) (OBBA) as guest ligand and sensitizer of the Tb(III) fluorescence. In the presence of NO_2^- the florescence of the NPs is quenched as a consequence of an energy transfer from Tb(III) to NO_2^-. The response of the nanoprobe decreases linearly with the increase of NO_2^- concentration from 0.3 μM to 470 μM. In a study described by Qiu and coworkers, bimetal NCPs of Tb(III) and Ce(III) acted as a selective fluorescent probe for sensing of H_2O_2.[75] The NCP network is formed using Tb(III) and Ce(III) and adenosine triphosphate (ATP) as the bridging ligand. The suitable emission energy of Ce(III) matching to the adsorption energy of Tb(III) allows an efficient energy transfer from Ce(III) to Tb(III), resulting in the characteristic fluorescent emission of Tb(III). This fluorescence can be switched off by oxidation of Ce(III) to Ce(IV) in the presence of H_2O_2, as a consequence of interrupting the energy transfer from Ce(III) to Tb(III). On the basis of this quenching mechanism, these nanoparticles are used to detect H_2O_2 in a wide range from 5 nM to 50 μM. If glucose oxidase is present in the system, glucose can be determined using this nanosensor. Similarly, Xiao and coworkers reported the use of bimetal NCPs of Tb(III) and Ce(III) as a selective fluorescent probe for ALP activity.[76] The NCP network is generated using Tb(III) and Ce(III) and nucleotide GMP as the bridging ligand. As previously disclosed, an efficient energy transfer from Ce(III) to Tb(III) causes the characteristic fluorescent emission of Tb(III). This luminescence can be quenched by destruction of the Tb-GMP bonds by a dephosphorylation process in the presence of ALP, interrupting the energy transfer from Ce(III) to Tb(III). Based on this quenching of fluorescence, these nanoparticles are used to detect ALP in serum samples in a remarkable range from 0.05 U/mL to 20 U/mL

In a study reported by Ye and coworkers, a combined strategy of sensitizing, quenching and enhancement of the fluorescence of Tb(III) (on-off-on switch) in NCPs is applied for

the selective sensing of histidine and cysteine.[77] Thus, the nanoparticles were formed by self-assembly of AMP with Tb(III), and 5-sulfosalicylic acid (SSA) as an auxiliary ligand sensitizer of the fluorescence of Tb(III). The fluorescence of the AMP-Tb-SSA network is quenched by Cu(II), but is significantly enhanced by His and Cys, leading to a specific fluorescence "turn-on" assay for these amino acids by using Cu/SSA/AMP-Tb as a sensing nanoplatform. The enhancement of fluorescence resulted proportional to concentrations of His and Cys in the range from 0.2 to 150 μM and 0.5 to 200 μM, respectively. A similar strategy based on sensitizing, quenching and enhancement of the fluorescence of Eu(III) and Tb(III) in binuclear NCPs nanoparticles was applied by Wu and coworkers for the selective sensing of the anthrax biomarker dipicolinic acid (DPA).[78] The nanoparticles are made with Tb(III) and Eu(III) and the nucleotide GMP as bridging ligand and sensitizer to promote the Tb(III) luminescence at 549 nm without affecting Eu(III). Interestingly, the fluorescent emission of Eu(III) also appears at 620 nm because an effective energy transfer from Tb(III) to Eu(III) takes place. Upon the addition of DPA, a robust coordination with Tb(III) occurs, blocking this energy transfer between metals, causing the emission intensity of Tb(III) to increase during which a gradual decrease in the corresponding emission of Eu(III) is observed. The relative emission intensity (I_{549}/I_{620}) showed a linear response toward DPA within a concentration range from 2 to 16 μM, thus originating in a dual emission luminescent nanoprobe for DPA. Remarkably, this sensor allowed for the real-time monitoring of DPA release from noninfectious spores of simulant bacteria for *B. anthracis*, *B. subtilis*.

Besides Tb(III), other lanthanide ions such as Eu(III) and Ce(III) have been used to generate nanoprobes based on NCPs. Among the Eu(III)-based examples, Qu and coworkers reported the use of NCPs composed of Eu(III) ions, GMP as constitutive ligand and 4 different encapsulated fluorescent dyes, for the construction of an artificial tongue (Figure 5).[79] Different metal ions interact distinctively with GMP, affecting in turn the fluorescence of the dyes, providing a fluorescent probe for the simultaneous sensing of several ions. In particular Ag(I) and Cu(II) concentrations can be univocally determined in a range from 0.1 to 50 μM.

Inset Figure 5 here

Figure 5. Example of Eu(III)-based NCPs for chemical sensing. NCPs composed of Eu(III) ions, GMP as constitutive ligand and 4 different encapsulated fluorescent dyes, constitute an artificial tongue. Reproduced from reference 79 with permission of the copyright holder.

Shi and coworkers described how NCPs composed of Eu(III) ions and fluorochrome riboflavin-5'-phosphate (RiP) as constitutive bridging ligand can act as a nanosensor for anthrax biomarker DPA.[80] RiP in solution has a strong fluorescence at 536 nm but in the NCPs network this fluorescent emission decreases. Upon addition of DPA, the NCPs are broken, as a consequence of the strong interaction Eu(III) and DPA, resulting in the release of RiP and a concomitant enhancement of fluorescence, thus generating a nanosensor of DPA with a range of application between 0.04 and 1 μM.

Following another strategy, Chen and coworkers described how NCPs composed of Eu(III), and isophthalic acid (IPA) as main constitutive ligand and sensitizer of the fluorescence of Eu(III), constitute a switch-on fluorescence nanosensor for Hg(II).[81] The fluorescence of the NCP network is quenched in the presence of imidazole-4,5-dicarboxilic acid (Im) due to an inner filter effect (iFE) of this compound that absorbs part of the emission luminescence of Eu(III). Upon the addition of Hg(II), a significant enhancement of fluorescence takes place due to the disappearance of the iFE process as a consequence of the coordination of Hg(II) to Im. As nanosensor for Hg(II), it presents a remarkable range of application between 2 nM to 2 μM, including applications in biological fluids. Similarly, Xu and coworkers reported an example of Eu(III)-based NCPs nanoparticles acting as an efficient turn-on fluorescent nanoprobe for the detection of antibiotic ciprofloxacin.[82] In this case, the NCP network is formed with Eu(III) and GMP as bridging ligand. A fluorescent emission of Tb(III) occurs in the presence of ciprofloxacin, due to the formation of a complex between this compound and Eu(III) atoms. The thus obtained nanosensor presents a range of applications with linear enhancement of fluorescence between 1 to 40 μM. As previously referred, the anthrax biomarker DPA,[78] and alkaline phosphatase activity,[76] have also been the target of sensing by NCPs based on Eu(III) along with Tb(III). There are also several reported examples of using Ce(III)-based NCPs for chemical sensing. Thus, Qiu and coworkers described the use of fluorescent NCPs nanoparticles constructed by Ce(III), ATP as bridging ligand and units of tris(hydroxymethyl)aminomethane hydrochloric salt (Tris),

for hydrogen peroxide detection.[83] ATP sensitizes the fluorescence of Ce(III) but upon the addition of H_2O_2, part of Ce(III) atoms in the ATP-Ce-Tris network are oxidized to the Ce(IV) state, by which a quenching of the fluorescence occurs. The decrease of emission intensity showed a linear response towards H_2O_2 within a remarkable concentration range from 0.6 nM to 80 μM, thus originating a switch-off luminescent nanoprobe for H_2O_2. If coupled with the GOx enzyme, the sensor probed to be also effective for glucose sensing in a range between 0.1 μM to 100 μM.

Similarly, Lu and coworkers reported another switch-off fluorescent nanoprobe based on NCPs made of Ce(III), ATP as bridging ligand and Tris, for alkaline phosphatase activity sensing.[84] In this case, in the presence of the ALP enzyme the ATP phosphate bonds are hydrolyzed, leading to the dissociation of the NCPs network and eventually to a decrease of the fluorescence. The fluorescence quenching efficiency shows a linear relationship for ALP in a range from 0.1 to 10 mU mL^{-1} and can be used in human serum samples. Other nanoprobes made of NCPs based on Ce(III) have previously been reported in this section for the sensing of DNA,[71] H_2O_2,[75] and Hg(II),[69] in relation with Tb(III)-based nanosensors.

NCPs based on other ions different from lanthanide metals have also been described as sensors. Thus, NCPs with useful sensing properties based on Fe(III) originated in situ from the decomposition of Fe(II) present in the compound ferrocenedicarboxylic acid (FcDA) has been reported by Mao and coworkers. These authors described that the photodecomposition of FcDC in methanol produces electroactive NCPs particles.[85] Under exposition to natural light, partial decomposition of ferrocene dicarboxylate takes place, generating Fe(II) which is oxidized to give Fe(III) that in turn, coordinates with carboxylic acids present in the FcDA units, thus generating the NCPs network. The resulting nanoparticles showed interesting properties in the presence of O_2, as redox mediator in the reduction of O_2 to H_2O by the enzyme laccase. Tang and coworkers reported the use of bimetal Pt-Fe(III) NCPs for the sensing of the prostate specific antigen (PSA) used for prostate cancer prognosis.[86] In this case, previously formed Pt NPs are encapsulated in the process of formation of the NCPs network between molecules of ferrocene dicarboxylate and Fe(III) generated by partial photodecomposition of the FcDA. Next, these nanoparticles are conjugated to anti-

PSAantibody (Ab2) and deposited on an electrode surface functionalized with anti-PSAantibody (Ab1), generating a sandwich-type electrochemical immune sensor based on the capacity of the platinum particles for catalytic H_2O_2 reduction. Upon addition of H_2O_2 to the solution, a current resulted proportional to the logarithm of PSA concentration in a remarkable range from 0.001 to 60 ng/mL. Cu(II) has also been used as constitutive metal in several NCPs applied for sensing purposes. Thus, Zhou and coworkers described the use of NCPs nanorods made of Cu(II) and tyrosine or aspartic acid as bridging ligands as enzyme-free electrochemical biosensor for H_2O_2.[87] The material deposited on an electrode surface showed fast amperometic response in the presence of H_2O_2 in the range between 0.04 and 6.3 mM. Gai and coworkers reported NCPs, constructed by Cu(II) and GMP as bridging ligand, for H_2O_2 detection.[88] In solution, the particles were able to oxidize 3,3',5,5'-tetramethylbenzidine (TMB) to a blue colored product in the presence of H_2O_2, generating a colorimetric H_2O_2 assay based on the absorbance at 652 nm, in the range between 20 to 160 μM. If coupled with the GOx enzyme, the sensor probed to be also effective for glucose sensing ranging from 25 μM to 100 μM. In the case of Zn(II), Mao and coworkers described the use of NCPs made of Zn(II), 1,4-bis(imidazole-1-ylmethyl)benzene (bix) as bridging ligand, and the encapsulated dye Rhodamine B (RhB), as a colorimetric and fluorescent dual mode sensor to measure the alcohol content in spirit samples.[21] In this case, the RhB-Zn(bix) nanoparticles are stable in pure alcohol, but upon the progressive addition of water the Zn(bix) network is destroyed, resulting in the release of RhB which confers color and fluorescent properties to the solution, constituting a colorimetric and fluorescent dual mode sensing of the alcohol strength, in a range between 20 and 100% where the values of real samples fall. Following a similar strategy, Cao and coworkers demonstrated the utility of NCPs composed of Zn(II), biphenyl-4,4'-dicarboxilic acid (BDA) as main constitutive ligand, and encapsulated fluorophore rhodamine B and quencher methylene blue, as a turn-on fluorescent nanosensor for phosphate in human serum.[89] The nanoparticles are disassembled in the presence of phosphate owing to the strong coordination between zinc and phosphate, liberating RhB into solution and triggering the corresponding fluorescence response, thus generating a switch-on fluorescent probe for PO_4^{3-} in a range between 0.5 and 50 μM in human serum samples.

Other metals have been used as constitutive part of NCPs, but only in single examples. Co(II) in combination with 3,5-diterbutylcatechol and bix as constitutive ligands, was reported by Zhou and coworkers to form NCPs used as a colorimetric and fluorescence dual sensor for hypochlorite ions.[90] Similarly to other studies using different metals, the liberation of encapsulated RhB upon the degradation of the nanoparticles by the influence of an analyte, generates a switch-on probe of it. In this case, ClO⁻ destroys the NCPs network, liberating RhB and enhancing both color and fluorescence of the solution in a linear range from 1 to 400 μM of ClO⁻. Ye and coworkers described the use of nickel-based NCPs as sacrificial template for the synthesis of nickel oxide nanostructures used as part of an urease-based bio-electrode for urea sensing.[91] The NCPs are made with Ni(II) and benzene-1,4-dicarboxylic acid as constitutive bridging ligand. The prepared bio-electrode showed a linear response over the physiological range of urea concentration from 1.33 to 3.33 mM. Shen and coworkers reported the construction of a biosensor for glucose, using a modified electrode with glucose oxidase immobilized in a layer of Au-Ag-Pt core-shell nanoparticles, previously coated with a NCPs network formed between the Ag of the nanoparticles, H_2PtCl_6 and the ligand 2,5-dimercapto-1,3,4-thiadiazole.[92] The obtained biosensor showed a remarkable range for glucose sensing from 0.5 μM to 3.33 mM.

4. Perspectives

In spite of being at relative early stages of development (this novel family of nanoparticles was described for the first time 15 years ago), the results so far obtained in areas such as Nanomedicine and Sensors are really exciting. These nanoparticles do not exhibit an open-framework structure, but they can encapsulate different drugs with very high yields through both chemical and physical entrapment. Accordingly, different release routes have been explored such that the drugs have IC_{50} values similar to those of the free drug, even higher, while minimizing side effects. Moreover, it has already been shown that the coordination framework does not exhibit any toxicity (whenever the proper choice of metal ions and ligands are made). The chemical flexibility of these nanoparticles also allow for the fabrication of smart nanoparticles that respond to different external stimuli. Upon exposure to a given physiological media, the active units

are released to the media showing suitable efficiencies. This is one of the challenges followed nowadays in the field of drug release as ON/OFF systems are expected to significantly decrease undesired toxicities. The use of NCPs as platforms for chemical sensing has also grown exponentially over the last years. Lanthanide-based NCPs nanoparticles constitute without any doubt the main family of NCPs used as sensors for different chemical species; mainly, the fluorescence of a sample is enhanced or quenched in the absence/presence of a certain analyte. Therefore, NCPs offer a significant versatility and variety to develop new materials with ever-improved properties thanks to the countless combinations provided by coordination chemistry.

Even though successful, there are still a lot of issues to be addressed, among them:

- To understand the mechanisms that control the release of the drugs. For this, it is required to gain more control over the kinetics of: i) diffusion, ii) degradation of the nanostructure (which does not necessarily involve chemical degradation) or iii) a combination of both. Diffusion-induced delivery is modulated mainly by host-guest interactions, whereas degradation-induced diffusion through nanoparticle-body fluid interactions.

- Another challenge to be faced in the near future is the fabrication of stable and monodisperse colloidal solutions by controlling the nature of the metal ions and ligands (though this approach could be limited by the need to incorporate active drugs) or surface modification. This last approach is expected to be more successful thanks to its inherent chemical flexibility and the surface modification of the nanoparticles with other active units such as fluorophores, PEG or even antibodies.

- Finally, further studies yielding insight into their bio-distribution and bio-degradation mechanisms are required. Development of proper pharmacokinetic profiles will be another major step. If successful, NCPs perform both detection and efficacy of a given therapy, foundational perspectives for "theranostics" or personalized therapy.

5. Acknowledgments

6. References

1. Chen, L. J.; Yang, H. B. *Acc. Chem. Res.* **2018**, *51*, 2699–2710.

2. Lin, W.; Rieter, W. J.; Taylor, K. M. L. *Angew. Chem. Int. Ed.* **2009**, *48*, 650–658.

3. Spokoyny, A. M.; Kim, D.; Sumrein, A.; Mirkin, C. A. *Chem. Soc. Rev.* **2009**, *38*, 1218–1227.

4. Lee, H. J.; Cho, Y. J.; Cho, W.; Oh, M. *ACS Nano* **2013**, *7*, 491–499.

5. Dang, S.; Zhu, Q. L.; Xu, Q. *Nat. Rev. Mater.* **2017**, *3*.

6. a) Lan, G.; Ni, K.; Lin, W. *Coord. Chem. Rev.* **2019**, *379*, 65–81. b) Lu, K.; Aung, T.; Guo, N.; Weichselbaum, R.; Lin, W. *Adv. Mater.* **2018**, *30*, 1–20.

7. Adarsh, N. N.; Novio, F.; Ruiz-Molina, D. *Dalt. Trans.* **2016**, *45*, 11233–11255.

8. Guardingo, M.; Busqué, F.; Ruiz-Molina, D. *Chem. Commun.* **2016**, *52*, 11617–11626.

9. Bousseksou, A.; Molnár, G.; Salmon, L.; Nicolazzi, W. *Chem. Soc. Rev.* **2011**, *40*, 3313–3335.

10. Puigmartí-Luis, J. *Chem. Soc. Rev.* **2014**, *43*, 2253–2271.

11. a) Guardingo, M.; González-Monje, P.; Novio, F.; Bellido, E.; Busqué, F.; Molnár, G.; Bousseksou, A.; Ruiz-Molina, D. *ACS Nano* **2016**, *10*, 3206–3213. b) Bellido, E.; González-Monje, P.; Guardingo, M.; Novio, F.; Sánchez, A.; Montero, M.; Molnar, G.; Bousseksou, A.; Ruiz-Molina, D. *RSC Adv.* **2016**, *6*, 76666–76672.

12. Oh, M.; Mirkin, C. a. *Nature* **2005**, *438*, 651–654.

13. Sun, X.; Dong, S.; Wang, E. *J. Am. Chem. Soc.* **2005**, *127*, 13102–13103.

14. Park, K. H.; Jang, K.; Son, S. U.; Sweigart, D. A. *J. Am. Chem. Soc.* **2006**, *128*, 8740–8741.

15. a) Forestier, T.; Mornet, S.; Daro, N.; Nishihara, T.; Mouri, S.; Tanaka, K.; Fouché, O.; Freysz, E.; Létard, J.-F. *Chem. Commun.* **2008**, *36*, 4327-4329. b) Volatron, F.; Catala, L.; Rivière, E.; Gloter, A.; Stéphan, O.; Mallah, T. *Inorg. Chem.* **2008**, *47*, 6584–6586. c) Boldog, I.; Gaspar, A. B.; Martínez, V.; Pardo-Ibañez, P.; Ksenofontov, V.; Bhattacharjee, A.; Gütlich, P.; Real, J. A. *Angew. Chem. Int. Ed.* **2008**, *47*, 6433–6437. d) Coronado, E.; Galán-Mascarós, J. R.; Monrabal-Capilla, M.; García-Martínez, J.; Pardo-Ibáñez, P. *Adv. Mater.* **2007**, *19*, 1359–1361. e) Galán-Mascarós, J. R.; Coronado, E.; Forment-Aliaga, A.; Monrabal-Capilla, M.; Pinilla-Cienfuegos, E.; Ceolin, M. *Inorg. Chem.* **2010**, *49*, 5706–5714.

16 Novio, F.; Ruiz-Molina, D. *RSC Adv.* **2014**, *4*, 15293–15296.

17. a) Rieter, W. J.; Taylor, K. M. L.; An, H.; Lin, W.; Lin, W. *J. Am. Chem. Soc.* **2006**, *128*, 9024–9025. b) Taylor, K. M. L.; Rieter, W. J.; Lin, W. Bin. *J. Am. Chem. Soc.* **2008**, *130*, 14358–14359.

18. Nador, F.; Novio, F.; Ruiz-Molina, D. *Chem. Commun.* **2014**, *50*, 14570–14572.

19. Jeon, Y. M.; Armatas, G. S.; Heo, J.; Kanatzidis, M. G.; Mirkin, C. A. *Adv. Mater.* **2008**, *20*, 2105–2110.

20. González-Monje, P.; Novio, F.; Ruiz-Molina, D. *Chem. Eur. J.* **2015**, *21*, 10094–10099.

21. Deng, J.; Ma, W.; Yu, P.; Mao, L. *Anal. Chem.* **2015**, *87*, 6958–6965.

22. a) Hu, M.; Belik, A. A.; Imura, M.; Mibu, K.; Tsujimoto, Y.; Yamauchi, Y. *Chem. Mater.* **2012**, *24*, 2698–2707. b) Wang, K.; Geng, Z.; Zheng, M.; Ma, L.; Ma, X.; Wang, Z. *Cryst. Growth Des.* **2012**, *12*, 5606–5614. c) Shahverdizadeh, G. H.; Masoudian, S.; Soudi, A. A.; Bigdeli, F.; Monfared, H. H.; Morsali, A.; Khavasi, H. R. *J. Inorg. Organomet. Polym.* **2011**, *21*, 171–174.

23. a) Guardingo, M.; Busqué, F.; Novio, F.; Ruiz-Molina, D. *Inorg. Chem.* **2015**, *54*, 6776–6781. b) Imaz, I.; Maspoch, D.; Rodríguez-Blanco, C.; Pérez-Falcón, J. M.; Campo, J.; Ruiz-Molina, D. *Angew. Chem. Int. Ed.* **2008**, *47*, 1857–1860.

24. Amorín-Ferré, L.; Busqué, F.; Bourdelande, J. L.; Ruiz-Molina, D.; Hernando, J.; Novio, F. *Chem. Eur. J.* **2013**, *19*, 17508–17516.

25. a) Imaz, I.; Hernando, J.; Ruiz-Molina, D.; Maspoch, D. *Angew. Chem. Int. Ed.* **2009**, *48*, 2325–2329; b) Imaz, I.; Rubio-Martínez, M.; García-Fernández, L.; García, F.; Ruiz-Molina, D.; Hernando, J.; Puntes, V.; Maspoch, D. *Chem. Commun.* **2010**, *46*, 4737–4739.

26. Rieter, W. J.; Pott, K. M.; Taylor, K. M. L.; Lin, W. *J. Am. Chem. Soc.* **2008**, *130*, 11584–11585.

27. Solórzano, R.; Tort, O.; García-Pardo, J.; Escribà, T.; Lorenzo, J.; Arnedo, M.; Ruiz-Molina, D.; Alibés, R.; Busqué, F.; Novio, F *Biomaterials Science* **2019**, *7*, 178-186

28. Novio, F.; Simmchen, J.; Vázquez-Mera, N.; Amorín-Ferré, L.; Ruiz-Molina, D. *Coord. Chem. Rev.* **2013**, *257*, 2839–2847.

29. Novio, F.; Lorenzo, J.; Nador, F.; Wnuk, K.; Ruiz-Molina, D. *Chem. Eur. J.* **2014**, *20*, 15443–15450.

30. Liang, G.; Ni, H.; Bao, S.; Zhu, F.; Gao, H.; Wu, Q. *J. Phys. Chem. B* **2014**, *118*, 6339–6345.

31. Yan, X.; Li, Y.; Zou, Q.; Yuan, C.; Li, S.; Xing, R. *Angew. Chem. Int. Ed.* **2018**, *57*, 17084–17088.

32. Li, M.; Wang, C.; Di, Z.; Li, H.; Zhang, J.; Xue, W.; Zhao, M.; Zhang, K.; Zhao, Y.; Li, L. *Angew. Chem. Int. Ed.* **2019**, *58*, 1350–1354.

33. Fan, Z.; Sun, L.; Huang, Y.; Wang, Y.; Zhang, M. *Nat. Nanotechnol.* **2016**, *11*, 388–394.

34. Bertleff-Zieschang, N.; Rahim, M. A.; Ju, Y.; Braunger, J. A.; Suma, T.; Dai, Y.; Pan, S.; Cavalieri, F.; Caruso, F. *Chem. Commun.* **2017**, *53*, 1068–1071.

35. Gao, P. F.; Zheng, L. L.; Liang, L. J.; Yang, X. X.; Li, Y. F.; Huang, C. Z. *J. Mater. Chem. B* **2013**, *1*, 3202–3208.

36. Bai, L.; Song, F.; Wang, X. H.; Cao, J. Y. Q.; Han, X.; Wang, X. L.; Wang, Y. Z. *RSC Adv.* **2015**, *5*, 47629–47639.

37. Han, K.; Zhang, W. Y.; Zhang, J.; Ma, Z. Y.; Han, H. Y. *Adv. Healthc. Mater.* **2017**, *6*, 1–9.

38. Xu, S.; Liu, J.; Li, D.; Wang, L.; Guo, J.; Wang, C.; Chen, C. *Biomaterials* **2014**, *35*, 1676–1685.

39. Wang, T.; Liu, X.; Zhu, Y.; Cui, Z. D.; Yang, X. J.; Pan, H.; Yeung, K. W. K.; Wu, S. *ACS Biomater. Sci. Eng.* **2017**, *3*, 816–825

40. Ejima, H.; Richardson, J. J.; Liang, K.; Best, J. P.; Van Koeverden, M. P.; Such, G. K.; Cui, J.; Caruso, F. *Science* **2013**, *341* (6142), 154–157.

41. Rahim, M. A.; Ejima, H.; Cho, K. L.; Kempe, K.; Müllner, M.; Best, J. P.; Caruso, F. *Chem. Mater.* **2014**, *26*, 1645–1653.

42. Ping, Y.; Guo, J.; Ejima, H.; Chen, X.; Richardson, J. J.; Sun, H.; Caruso, F. *Small* **2015**, *11*, 2032–2036.

43. Ju, Y.; Cui, J.; Sun, H.; Müllner, M.; Dai, Y.; Guo, J.; Bertleff-Zieschang, N.; Suma, T.; Richardson, J. J.; Caruso, F. *Biomacromolecules* **2016**, *17*, 2268–2276.

44. Ju, Y.; Dai, Q.; Cui, J.; Dai, Y.; Suma, T.; Richardson, J. J.; Caruso, F. *ACS Appl. Mater. Interfaces* **2016**, *8*, 22914–22922.

45. Park, J. H.; Kim, K.; Lee, J.; Choi, J. Y.; Hong, D.; Yang, S. H.; Caruso, F.; Lee, Y.; Choi, I. S. *Angew. Chem. Int. Ed.* **2014**, *53*, 12420–12425.

46. Besford, Q. A.; Ju, Y.; Wang, T. Y.; Yun, G.; Cherepanov, P. V.; Hagemeyer, C. E.; Cavalieri, F.; Caruso, F. *Small* **2018**, *14*, 1–9.

47. Huang, W.; Hao, P.; Qin, J.; Luo, S.; Zhang, T.; Peng, B.; Chen, H.; Zan, X. Hexahistidine-*Acta Biomater.* **2019**, *90,* 441–452.

48. Liu, J.; Wang, H.; Yi, X.; Chao, Y.; Geng, Y.; Xu, L.; Yang, K.; Liu, Z. *Adv. Funct. Mater.* **2017**, *27*, 1–10.

49. Liu, J.; Tian, L.; Zhang, R.; Dong, Z.; Wang, H.; Liu, Z. *ACS Appl. Mater. Interfaces* **2018**, *10*, 43493–43502.

50. Yang, Y.; Xu, L.; Zhu, W.; Feng, L.; Liu, J.; Chen, Q.; Dong, Z.; Zhao, J.; Liu, Z.; Chen, M. *Biomaterials* **2018**, *156*, 121–133.

51. Wang, B.; Jacquet, M.; Wang, K.; Xiong, K.; Yan, M.; Courtois, J.; Royal, G *New J. Chem.* **2018**, *42*, 7823–7829.

52. Zhang, Y.; Guo, Y.; Wu, S.; Liang, H.; Xu, H. *ACS Omega* **2017**, *2*, 2536–2543.

53. Liu, J.; Yang, G.; Zhu, W.; Dong, Z.; Yang, Y.; Chao, Y.; Liu, Z. *Biomaterials* **2017**, *146*, 40–48.

54. Hu, X. G.; Li, X.; Yang, S. I. Novel Photochromic Infinite Coordination Polymer Particles Derived from a Diarylethene Photoswitch. *Chem. Commun.* **2015**, *51*, 10636–10639.

55. Cherepanov, P. V.; Rahim, M. A.; Bertleff-Zieschang, N.; Sayeed, M. A.; O'Mullane, A. P.; Moulton, S. E.; Caruso, F. *ACS Appl. Mater. Interfaces* **2018**, *10*, 5828–5834.

56. Buwalda, S.; Nottelet, B.; Bethry, A.; Kok, R. J.; Sijbrandi, N.; Coudane, J. *J. Colloid Interface Sci.* **2019**, *535*, 505–515.

57. Li, S.; Zou, Q.; Li, Y.; Yuan, C.; Xing, R.; Yan, X. *J. Am. Chem. Soc.* **2018**, *140*, 10794–10802.

58. Liu, J.; Chen, Q.; Zhu, W.; Yi, X.; Yang, Y.; Dong, Z.; Liu, Z. *Adv. Funct. Mater.* **2017**, *27*, 10.

59. Wang, Y.; Wu, Y.; Li, F.; Chen, D. *Inorg. Chem. Commun.* **2014**, *40*, 143–147.

60. Pu, F.; Ju, E.; Ren, J.; Qu, X. *Adv. Mater.* **2014**, *26*, 1111–1117.

61. Pu, F.; Ren, J.; Qu, X. *ACS Appl. Mater. Interfaces* **2014**, *6*, 9557–9562.

62. Gao, R.-R.; Shi, S.; Li, Y.-J.; Wumaier, M.; Hu, X.-C.; Yao, T.-M. *Nanoscale* **2017**, *9*, 9589–9597.

63. Bai, L.; Wang, X. H.; Song, F.; Wang, X. L.; Wang, Y. Z. *Chem. Commun.* **2015**, *51*, 93–96.

64. Tan, H.; Liu, B.; Chen, Y. *ACS Nano* **2012**, *6*, 10505–10511.

65. Zhang, M.; Qu, Z.-B.; Han, C.-M.; Lu, L.-F.; Li, Y.-Y.; Zhou, T.; Shi, G. *Chem. Commun.* **2014**, *50*, 12855–12858.

66. Tan, H.; Zhang, L.; Ma, C.; Song, Y.; Xu, F.; Chen, S.; Wang, L. *ACS Appl. Mater. Interfaces.* **2013**, *5*, 11791–11796.

67. Lin, N.; Zhang, Q.; Xia, X.; Liang, M.; Zhang, S.; Cao, Q.; Ding, Z. A *RSC. Adv.* **2017**, *7*, 21446–21451.

68. Deng, J.; Yu, P.; Wang, Y.; Mao, L. *Anal. Chem.* **2015**, *87*, 3080–3086.

69. Zhang, Z.; Wu, Y.; He, S.; Mao, L.; Xu, Y.; Li, G.; Ye, B. *Anal. Chim. Acta* **2018**, *1014*, 85-90.

70. Ou-Yang, J.; Li, C.-Y.; Li, Y.-F.; Yang, B.; Li, S.-J. *Sens. Actuators B* **2018**, *255*, 3355-3363.

71. Wang, F.; Liu, B.; Huang, P. J.; Liu, J. *Anal. Chem.* **2013**, *85*, 12144-12155.

72. Tan, H.; Ma, C.; Li, Q.; Wang, L.; Xu, F.; Chen, S.; Song, Y. *Analyst.* **2014**, *139*, 5516 5522.

73. Huang, P.; Wu, F.; Mao, L. *Anal. Chem.* **2015**, *87*, 6834-6841.

74. Qi, Z.; You, Q.; Chen, Y. *Anal. Chim. Acta* **2016**, *902*, 168-173.

75. Zeng, H.-H.; Zhang, L.; Rong, L.-Q.; Liang, R.-P.; Qiu, J.-D. A *Biosens. Bioelectron.* **2017**, *89*, 721-727.

76. Wang, F.; Hu, X.; Hu, J.; Peng, Q.; Zheng, B.; Du, J.; Xiao, D. *J. Mater. Chem. B* **2018**, *6*, 6008-6015.

77. Zhang, Z.; Wang, L.; Li, G.; Ye, B. *Analyst.* **2017**, *142*, 1821-1826.

78. Gao, N.; Zhang, Y.; Huang, P.; Xiang, Z.; Wu, F.-Y.; Mao, L. *Anal. Chem.* **2018**, *90*, 7004-7011.

79. Pu, F.; Ran, X.; Ren, J.; Qu, X. *Chem. Commun.* **2016**, *52*, 3410-3413.

80. Xue, S.-F.; Zhang, J.-F.; Chen, Z.-H.; Han, X.-Y.; Zhang, M.; Shi, G. *Anal. Chim. Acta* **2018**, *1012*, 74-81.

81. Li, Q.; Wang, C.; Tan, H.; Tang, G.; Gao, J.; Chen, C.-H. A *RSC Adv.* **2016**, *6*, 17811-17817.

82. Liu, B.; Huang, Y.; Shen, Q.; Zhu, X.; Hao, Y.; Qu, P.; Xu, M. *RSC Adv.* **2016**, *6*, 100743-100747.

83. Zeng, H.-H.; Qiu, W.-B.; Zhang, L.; Liang, R.-P.; Qiu, J.-D. *Anal. Chem.* **2016**, *88*, 6342-6348.

84. Chen, C.; Yuan, Q.; Ni, P.; Jiang, Y.; Zhao, Z.; Lu, Y. *Analyst* **2018**, *143*, 3821-3828.

85. Zhang, L.; Gao, X.; Yang, L.; Yu, P.; Mao, L. *ACS Appl. Mater. Interfaces* **2013**, *5*, 8120-8124.

86. Zhang, B.; Liu, B.; Chen, G.; Tang, D. *Biosens. Bioelectron.* **2015**, *64*, 6-12.

87. Zhou, B.; Xu, F.-C.; Yang, J.; Yao, J.; Xiao, Y.-H. *Mat. Lett.* **2013**, *107*, 206-209.

88. Hou, T.; Zhao, T.; Li, W.; Li, F.; Gai, P. *J. Mater. Chem. B* **2017**, *5*, 4607-4613.

89. Lin, N.; Li, J.; Lu, Z.; Bian, L.; Zheng, L.; Cao, Q.; Ding, Z. *Nanoscale* **2015**, *7*, 4971-4977.

90. Zhang, X.; Deng, J.; Shi, G.; Zhou, T. *RSC Adv.* **2015**, *5*, 107964-107969.

91. Mai, H. D.; Sung, G. Y.; Yoo, H. *RSC Adv.* **2015**, *5*, 78807-78814.

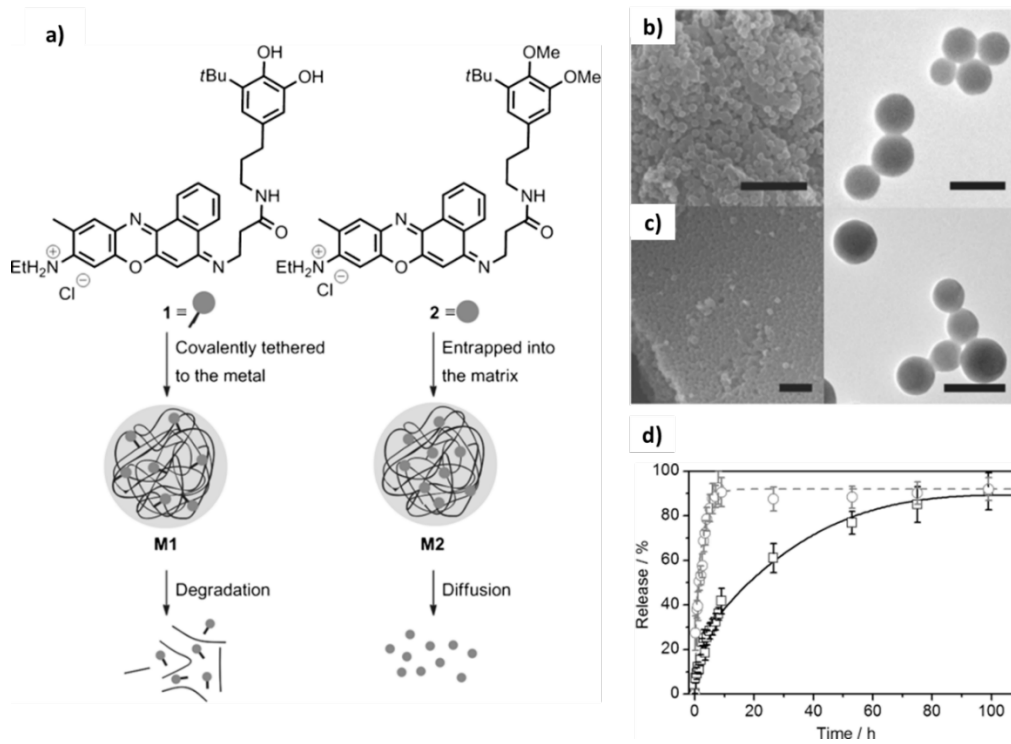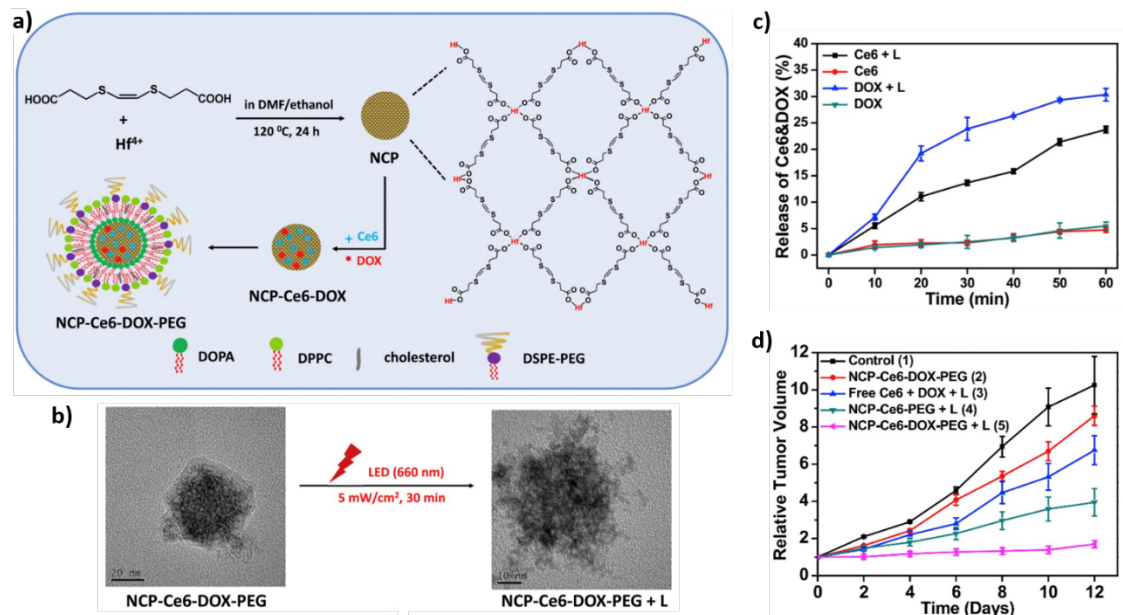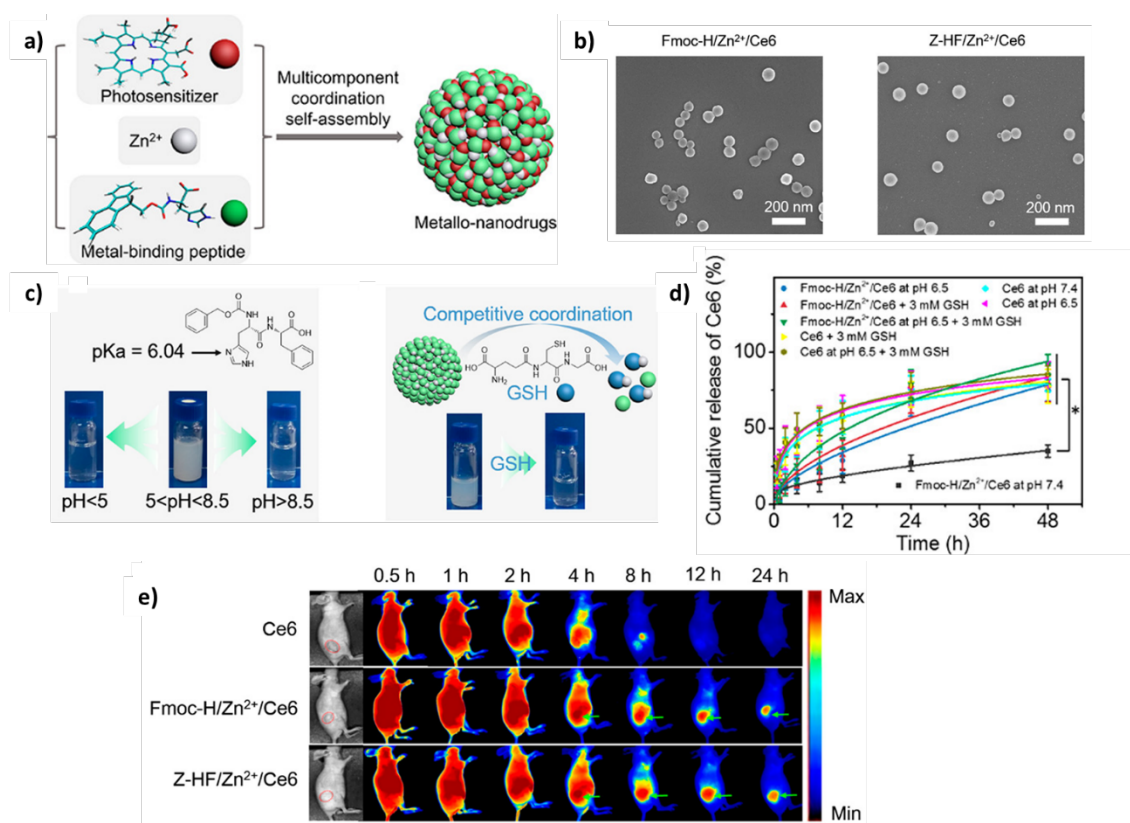92. Wang, L.; Zeng, Y.; Shen, A.; Fu, Y.; Zeng, L.; Hu, J. *RSC Adv.* **2016**, *6*, 86025-86033.
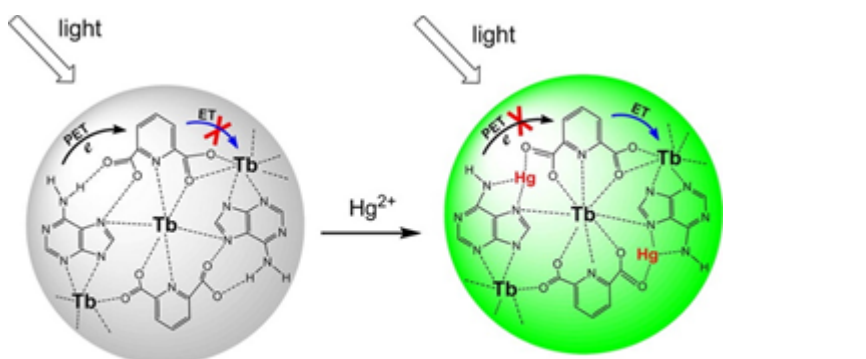
Figure 1

Figure 2

Figure 3

Figure 4

Figure 5